

# Distances to Dwarf Galaxies of the Canes Venatici I Cloud

D. I. Makarov,<sup>1,\*</sup> L. N. Makarova,<sup>1,†</sup> and R. I. Uklein<sup>1,‡</sup>

<sup>1</sup>*Special Astrophysical Observatory, Russian Academy of Sciences, Nizhnii Arkhyz, 369167 Russia*

We determined the spatial structure of the scattered concentration of galaxies in the Canes Venatici constellation. We redefined the distances for 30 galaxies of this region using the deep images from the Hubble Space Telescope archive with the WFPC2 and ACS cameras. We carried out a high-precision stellar photometry of the resolved stars in these galaxies, and determined the photometric distances by the tip of the red giant branch (TRGB) using an advanced technique and modern calibrations. High accuracy of the results allows us to distinguish the zone of chaotic motions around the center of the system. A group of galaxies around M 94 is characterized by the median velocity  $V_{LG} = 287$  km/s, distance  $D = 4.28$  Mpc, internal velocity dispersion  $\sigma = 51$  km/s and total luminosity  $L_B = 1.61 \times 10^{10} L_{\odot}$ . The projection mass of the system amounts to  $M_p = 2.56 \times 10^{12} M_{\odot}$ , which corresponds to the mass–luminosity ratio of  $(M/L)_p = 159 (M/L)_{\odot}$ . The estimate of the mass–luminosity ratio is significantly higher than the typical ratio  $M/L_B \sim 30$  for the nearby groups of galaxies. The CVnI cloud of galaxies contains 4–5 times less luminous matter compared with the well-known nearby groups, like the Local Group, M 81 and Centaurus A. The central galaxy M 94 is at least  $1^m$  fainter than any other central galaxy of these groups. However, the concentration of galaxies in the Canes Venatici may have a comparable total mass.

## I. INTRODUCTION

The distribution of nearby galaxies of the Local Volume in the sky reveals a significant concentration of objects in a small region located in the Canes Venatici constellation (Fig. 1). This feature has been noted by Karachentsev (1966) and de Vaucouleurs (1975) [1, 2]. This complex is mostly populated by dwarf galaxies of late morphological types. Two peaks are distinguished in the distribution of the line-of-sight velocities of galaxies in the sky region  $\alpha = (11.5, 14.0)$ ,  $\delta = (+20^{\circ}, +60^{\circ})$  (Fig. 2). The first peak located around  $V_{LG} = 300$  km/s corresponds to the CVnI cloud, while the CVnII concentration has an average velocity of about 560 km/s. The Canes Venatici I cloud clearly differs from the other nearby galaxy clusters, such as the Local Group, M 81 or the groups

---

\*Electronic address: dim@sao.ru

†Electronic address: lidia@sao.ru

‡Electronic address: uklein@sao.ru

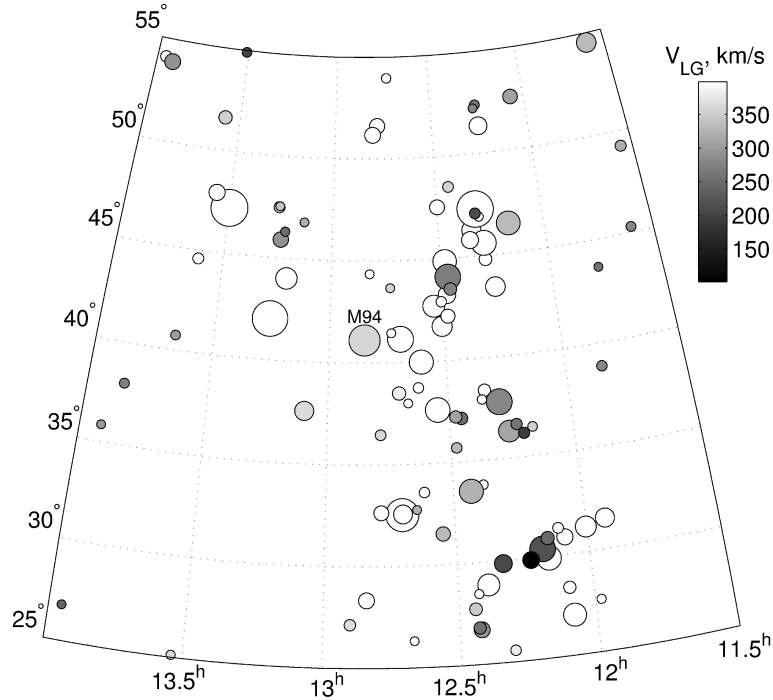


FIG. 1: The distribution of galaxies in the Canes Venatici constellation on the celestial sphere. The sizes of the circles are inversely proportional to the absolute magnitudes of objects. The line-of-sight radial velocities of the CVnI cloud galaxies with  $V_{LG} < 400$  km/s are shown by the shades of gray, while the white circles correspond to the galaxies of the distant background.

in the Centaurus by the absence of a clearly prominent gravitational center and looks diffuse. The concentration of galaxies in the Canes Venatici constellation has repeatedly attracted the attention of researchers. In the series of papers [3–6] the structure of the complex was studied by the photometry of the brightest blue stars in these galaxies. The use of the Hubble Space Telescope (HST) has significantly improved the distance accuracy and allowed to study the kinematics of the CVnI cloud of galaxies [7]. A blind survey of the sky in neutral hydrogen [8] was recently conducted in the region of nearby groups of galaxies in the Canes Venatici in order to study the functions of the HI-masses in dwarf galaxies. Only one object from this survey has no optical identification. In addition, Kaisin and Karachentsev [9] have investigated the current star formation of galaxies in the Canes Venatici according to the  $H\alpha$  survey data. The authors did not find any significant correlations between the star formation rates (SFR) in the galaxies and their neighborhood.

A rapid progress in the deep observations of the Canes Venatici galaxies, performed at the HST/ACS and HST/WFPC2, as well as a significant improvement of distance measurement by the tip of the red giant branch (TRGB) method allow us to refine the structure of this unusual

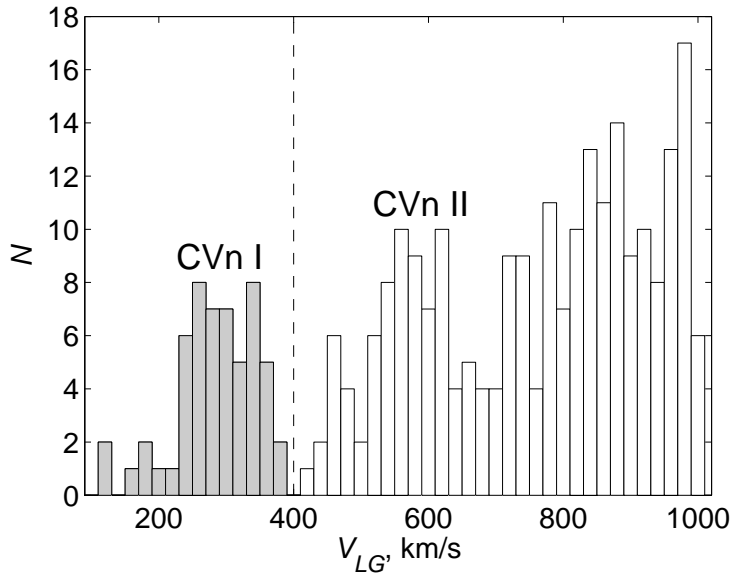


FIG. 2: The line-of-sight velocity distribution of galaxies in the direction of Canes Venatici constellation.

concentration of galaxies. In this paper, we determined the distances for 30 galaxies of the CVn I cloud, using the optimized TRGB method [10] and new zero point calibration [11].

## II. STELLAR PHOTOMETRY OF GALAXIES IN THE CANES VENATICI I CLOUD

The sample of galaxies from the Canes Venatici complex is presented in Table I. Direct images of the galaxies obtained with the ACS/HST and WFPC2/HST were taken from the archive of the Hubble Space Telescope. The images of all the galaxies were obtained in the F606W and F814W filters, with the exception of NGC 4214, which was observed in F555W and F814W. Standard initial reduction of images is done “on the fly.” Thus, the user gets the images with subtracted dark frames, flat field-corrected, and accounted for the presence of “bad” rows and some “hot”/“cold” pixels. The images of the studied galaxies are demonstrated in Fig. 3.

The photometry of resolved stars in the galaxies was performed using the HSTphot [27] and DOLPHOT [28] specialized software packages, developed for the PSF photometry in a crowded stellar field obtained with the WFPC2/HST and ACS/HST. The procedures of photometric reduction included masking the “bad” columns and pixels, removing the traces of cosmic ray particles from the images, and the simultaneous PSF photometry of the detected stars in two filters using the recommended parameters [27, 28]. Only the stars with photometry satisfying a number of quality criteria were used for the further measurements and analysis. Specifically, we selected the

TABLE I: Parameters of the HST observations for 30 galaxies of the Canes Venatici I cloud

Name	RA (J2000) Dec	Camera	Proposal	Filters	$T_{\text{exp}}$ , s
UGC 6541	113328.9+491418	WFPC2	8601	F814W/F606W	600/600
NGC 3738	113548.6+543122	ACS/WFC	12546	F814W/F606W	450/450
NGC 3741	113606.0+451708	WFPC2	8601	F814W/F606W	600/600
UGC 6817	115052.9+385251	WFPC2	8601	F814W/F606W	600/600
NGC 4068	120401.9+523519	ACS/WFC	9771	F814W/F606W	900/1200
NGC 4163	121209.2+361010	ACS/WFC	9771	F814W/F606W	900/1200
UGCA 276	121458.1+361306	WFPC2	8601	F814W/F606W	600/600
NGC 4214	121539.2+361939	WFPC2	6569	F814W/F555W	1300/1300
UGC 7298	121630.1+521340	WFPC2	8601	F814W/F606W	600/600
NGC 4244	121729.5+374826	ACS/WFC	10523	F814W/F606W	735/735
UGC 7559	122705.0+370836	WFPC2	8601	F814W/F606W	600/600
UGC 7577	122741.7+432939	WFPC2	8601	F814W/F606W	600/600
NGC 4449	122811.0+440535	WFPC2	5971	F814W/F606W	1400/1400
UGC 7605	122838.7+354304	WFPC2	8601	F814W/F606W	600/600
IC 3687	124215.1+383010	WFPC2	8601	F814W/F606W	600/600
KK 166	124913.1+353646	WFPC2	8601	F814W/F606W	600/600
M 94	125053.0+410712	ACS/WFC	10523	F814W/F606W	730/730
IC 4182	130549.6+373618	WFPC2	8584	F814W/F606W	2600/2600
UGC 8215	130803.6+464941	ACS/WFC	9771	F814W/F606W	900/1200
UGC 8308	131322.7+461913	WFPC2	8601	F814W/F606W	600/600
UGC 8320	131428.2+455511	WFPC2	8601	F814W/F606W	600/600
UGC 8331	131529.8+472959	ACS/WFC	10905	F814W/F606W	1148/938
NGC 5204	132936.5+582510	WFPC2	8601	F814W/F606W	600/600
UGC 8508	133044.4+545441	WFPC2	8601	F814W/F606W	600/600
UGC 8638	133919.6+244631	ACS/WFC	9771	F814W/F606W	900/1200
UGC 8651	133953.8+404421	ACS/WFC	10210	F814W/F606W	1209/1016
UGC 8760	135051.2+380116	ACS/WFC	10210	F814W/F606W	1189/998
UGC 8833	135448.5+355016	ACS/WFC	10210	F814W/F606W	1189/998
KK 230	140710.4+350340	ACS/WFC	9771	F814W/F606W	900/1200
UGC 9128	141556.5+230320	ACS/WFC	10210	F814W/F606W	1174/985

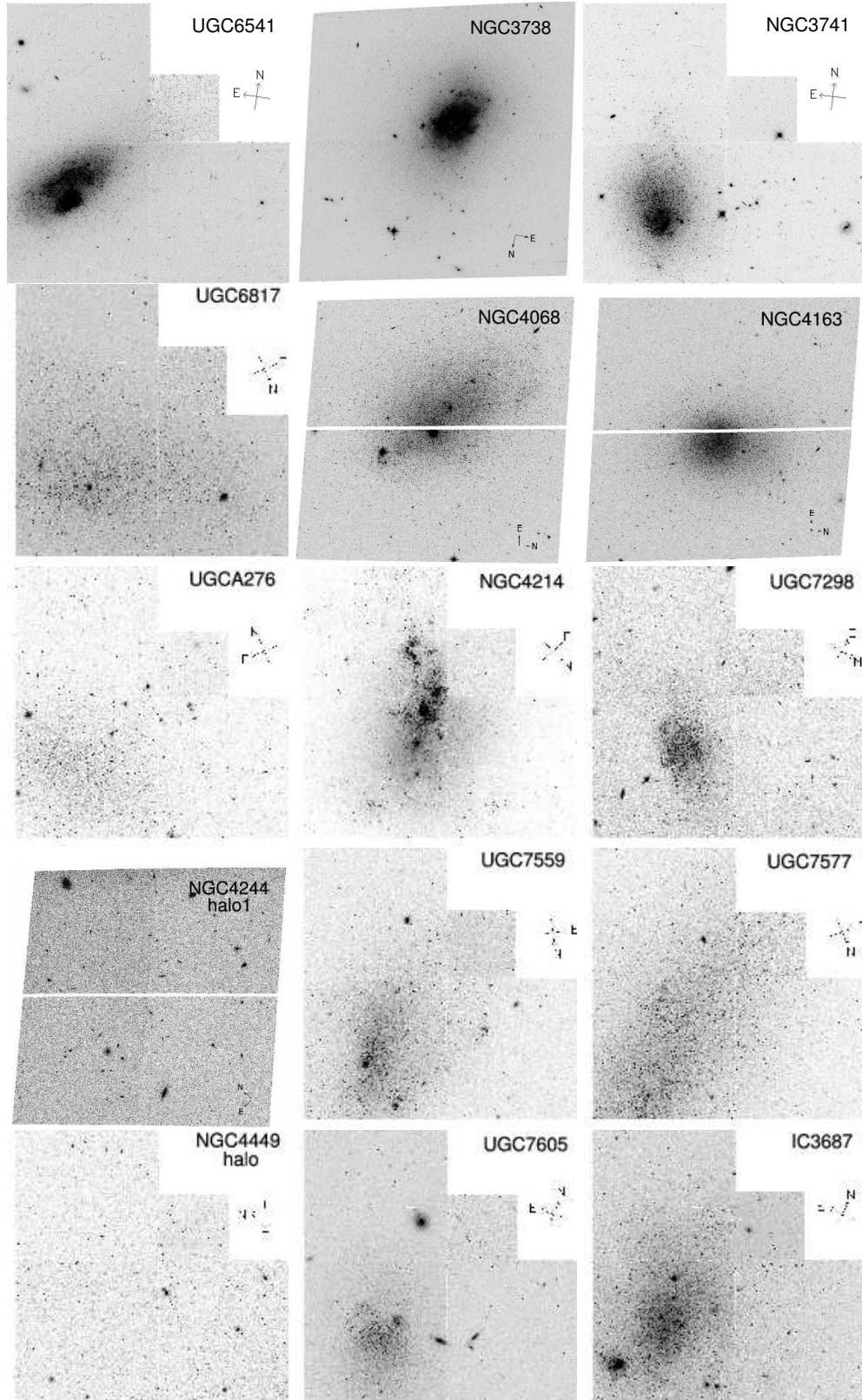


FIG. 3: The images of the studied galaxies in the Canes Venatici I cloud, obtained with the HST WFPC2 or ACS.

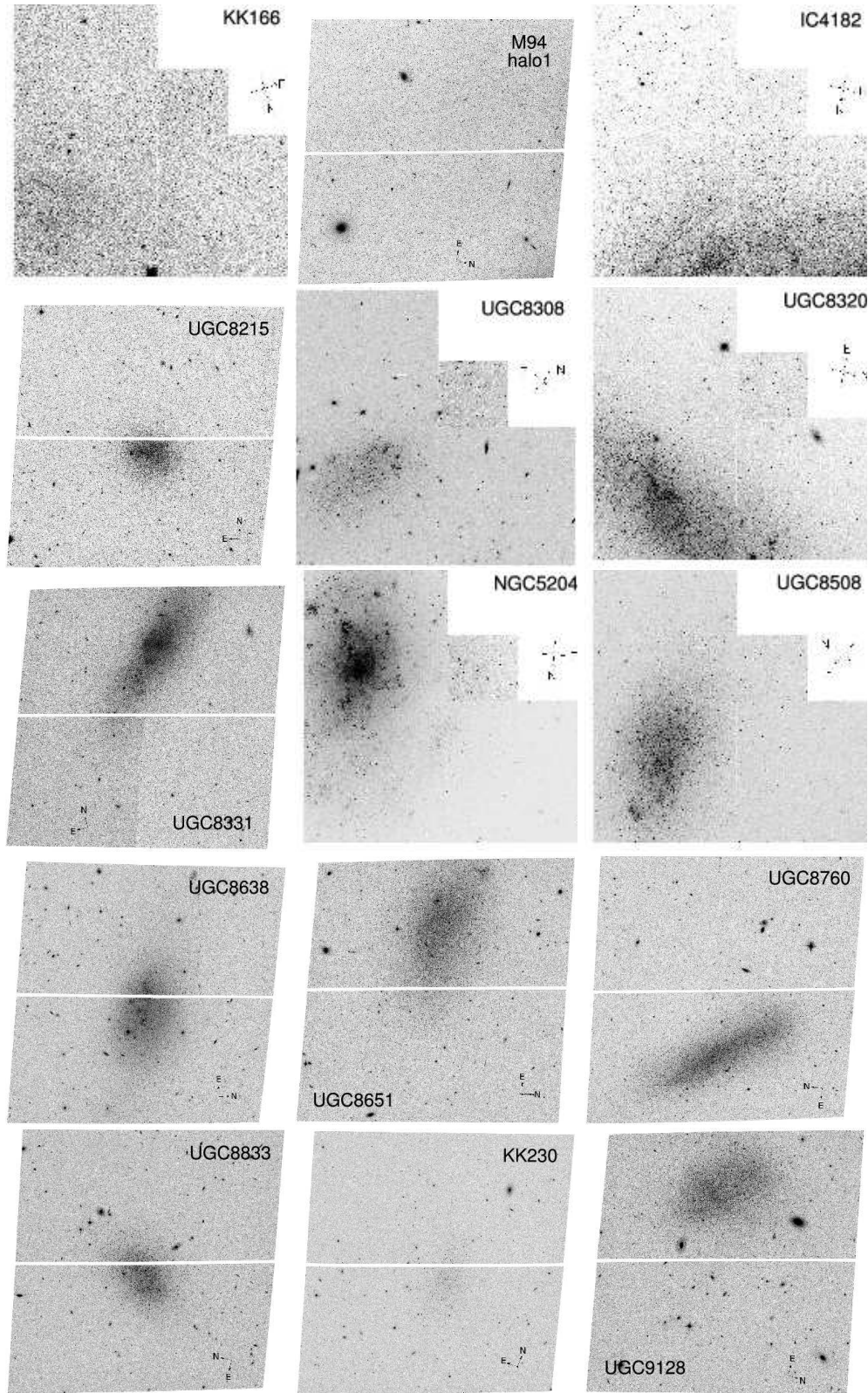


FIG. 3: (Contd.).

stars with the signal-to-noise ratio of  $S/N \geq 5$  in both filters,  $\chi^2 \leq 2.5$  and  $|\text{sharp}| \leq 0.3$ .

During the photometry, we paid special attention to the photometric errors. Since the quality of measurements in the crowded star fields is severely affected by the presence of close neighbors, we ran artificial star tests. We created a large library of artificial stars for each galaxy, the color–magnitude distribution of which would correspond to the actual one. Exactly the same photometry procedures were applied to these artificial stars in the galaxy images, as did the real stars. This time consuming process is the best way to estimate the real photometric errors, accounting for the incompleteness of photometry, very close neighbors, and superimposed stars.

### III. COLOR–MAGNITUDE DIAGRAMS

The color–magnitude diagrams (CMD) of stars from the studied galaxies are shown in Fig. 4. Irregular dwarf galaxies constitute the vast majority of objects in our sample. The upper part of the Main Sequence is clearly discernible in all the diagrams, it contains blue stars with the mean color index close to zero. The top right part of the CMD is occupied by red supergiants and the stars of the asymptotic giant branch (AGB), both these branches are populated differently for various galaxies. The largest population in each diagram is the RGB stars. We have selected from the Hubble archive only those exposures which are deep enough to safely identify the RGB in the galaxy, and therefore, determine its distance with a good accuracy by the TRGB method.

### IV. FINDING THE DISTANCES

To accurately determine the structure of the cloud of galaxies in the Canes Venatici constellation, we need to know the precise photometric distances to these galaxies, uniformly estimated. The distance estimates to many galaxies of the cloud were performed earlier, using the tip of the red giant branch method as one of the most accurate distance indicators. However, a uniform estimation of such distances is fulfilled for the first time. Moreover, an important factor for refining the distances is to improve the method itself, which was done by authors. In order to determine the TRGB values, we used our `TRGBT00L` code, based on the maximum likelihood algorithm for the luminosity function of stars in a galaxy, and taking into account accurate photometric errors, determined from artificial star tests [10]. The calibration of the TRGB method has been recently improved [11]. In that study, the color index–absolute TRGB magnitude dependence, as well as the zero-points of ACS and WFPS2 photometric systems were determined. The position of the

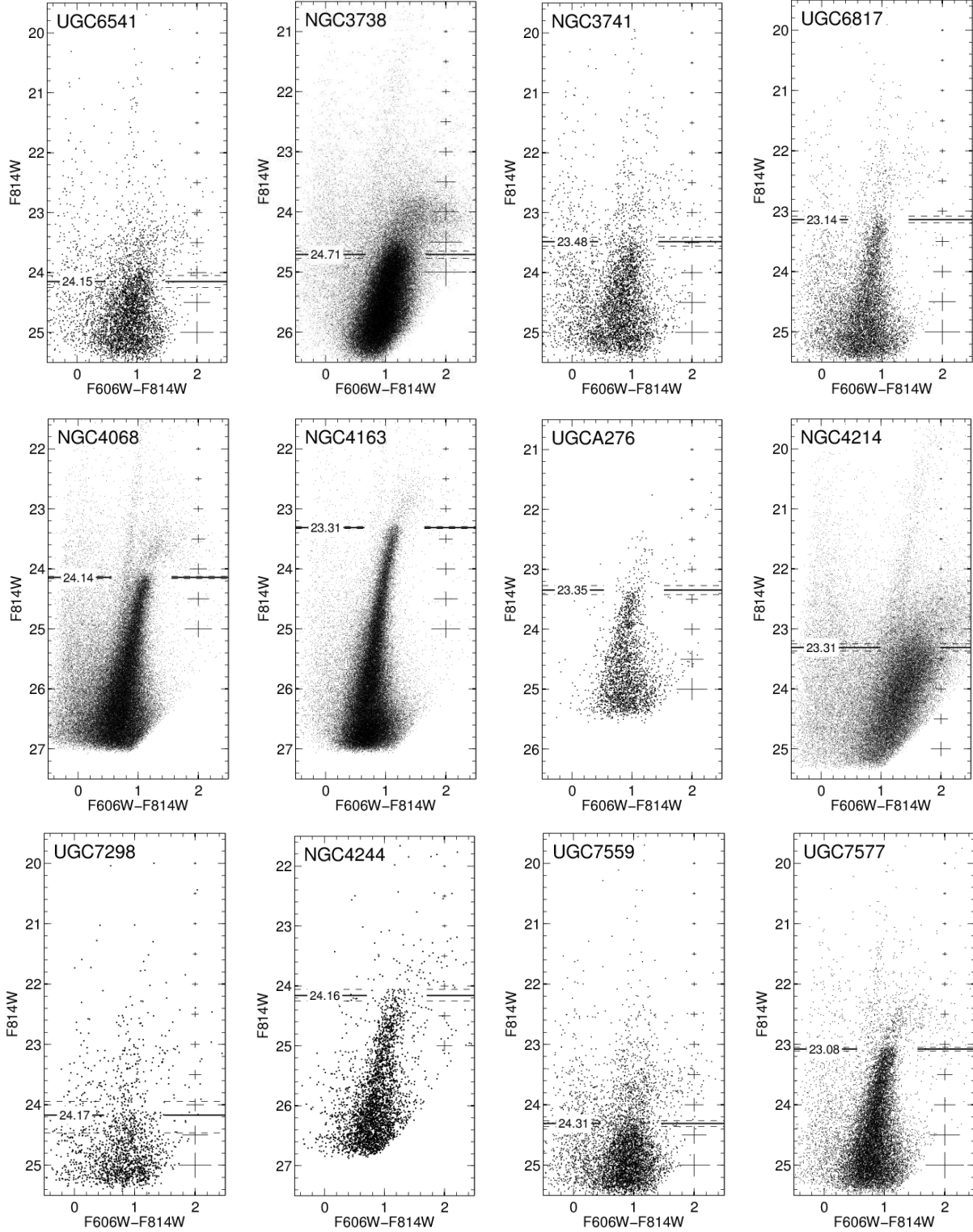


FIG. 4: The color-magnitude diagrams for the stars of the Canes Venatici I cloud galaxies. The crosses indicate the typical errors of stellar photometry. The TRGB position is indicated by the straight line, the corresponding measurement errors are depicted by the dashed lines.



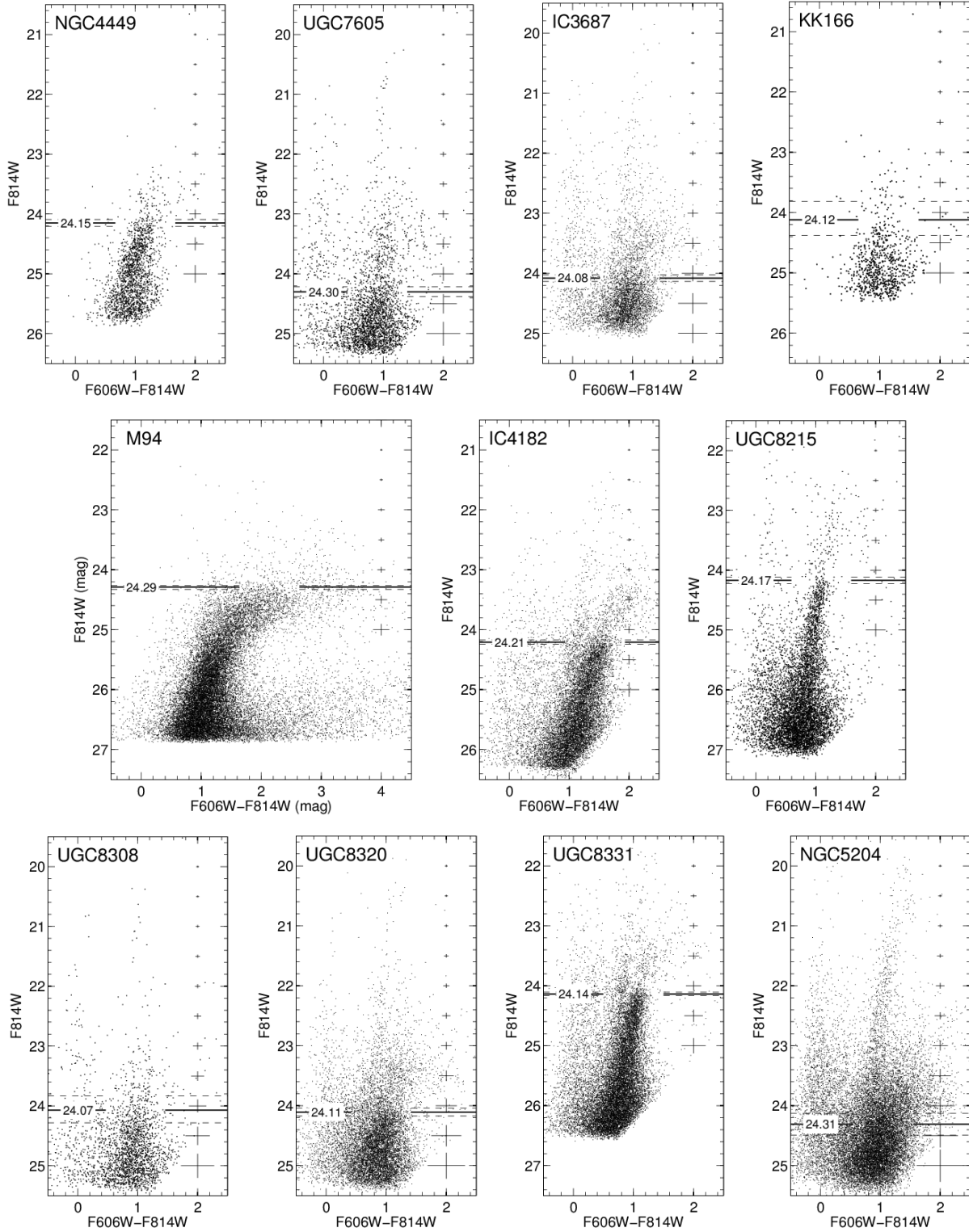


FIG. 4: (Contd.).

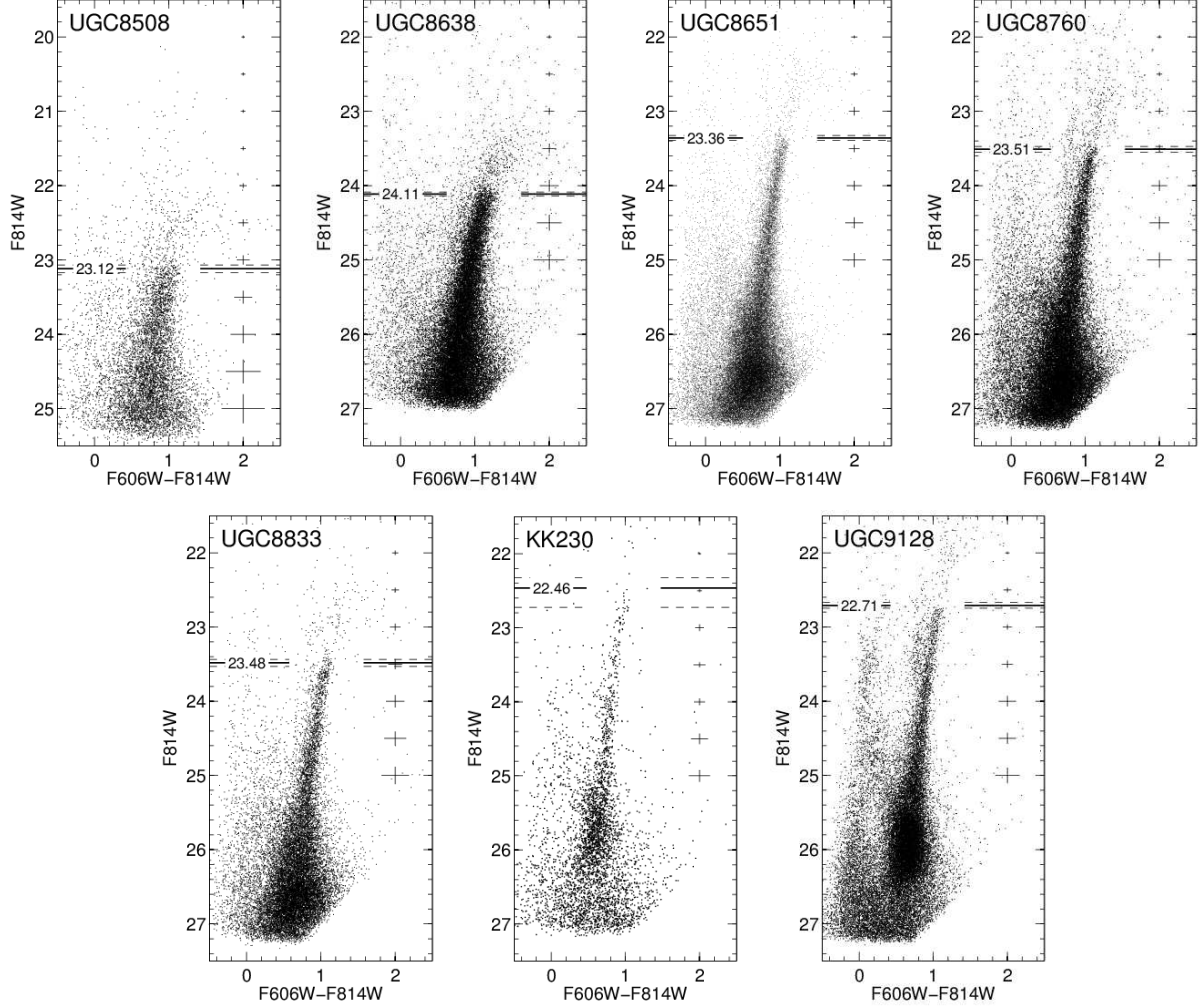


FIG. 4: (Contd.).

luminosity function cut-off and the corresponding  $1\sigma$  error are shown in the CMDs of the studied galaxies by horizontal lines (Fig. 4).

New photometric distances to the galaxies of the Canes Venatici I cloud are summarized in Table II. It lists: (1) the name of the galaxy in the known catalogs; (2) total apparent magnitude  $B_t$  in the  $B$ -band; (3) heliocentric velocity  $V_h$ ; (4) color excess  $E(B - V)$  in the direction of the galaxy according to [29]; (5) TRGB position, determined using the TRGBT00L; (6) the averaged color  $(F814W - F606W)_{\text{TRGB}}$  of stars in the TRGB region (for the NGC 4214 galaxy, we used the F555W filter instead of F606W); (7)  $(m - M)_0$  is the measured distance modulus of the galaxy in mag; (8)  $D$  is the corresponding photometric distance in Mpc; (9) the line-of-sight velocity relative to the centroid of the Local Group  $V_{\text{LG}}$ , according to [30]; (10)  $A_B^i$  is the internal absorption in the galaxy in the  $B$ -filter, according to [31]; (11)  $M_B$  is the absolute stellar B-magnitude of

TABLE II: The distances of galaxies in the CVnI cloud

Name	$B_t$ , <sup>*</sup> mag	$V_h$ , <sup>**</sup> km/s	$E(B - V)$ , mag	TRGB, <sup>***</sup> mag	Color, <sup>****</sup> mag	$(m - M)_0$ , mag	$D$ , Mpc	$V_{LG}$ , km/s	$A_B^i$ , mag	$M_B$ , mag	Ref
UGC 6541	14.44	249 ± 2	0.019	24.15 <sup>+0.10</sup> <sub>-0.10</sub>	0.977 <sup>+0.034</sup> <sub>-0.010</sub>	28.15 <sup>+0.12</sup> <sub>-0.12</sub>	4.26 <sup>+0.23</sup> <sub>-0.23</sub>	303	0.00	-13.79	<sup>b</sup> , <sup>A</sup>
NGC 3738	11.87	225 ± 8	0.010	24.71 <sup>+0.06</sup> <sub>-0.06</sub>	1.188 <sup>+0.004</sup> <sub>-0.004</sub>	28.76 <sup>+0.08</sup> <sub>-0.08</sub>	5.65 <sup>+0.22</sup> <sub>-0.22</sub>	306	0.02	-16.95	<sup>b</sup> , <sup>D</sup>
NGC 3741	14.40	229 ± 2	0.025	23.48 <sup>+0.07</sup> <sub>-0.07</sub>	0.937 <sup>+0.023</sup> <sub>-0.021</sub>	27.48 <sup>+0.09</sup> <sub>-0.09</sub>	3.13 <sup>+0.14</sup> <sub>-0.13</sub>	263	0.00	-13.18	<sup>b</sup> , <sup>A</sup>
UGC 6817	13.70	251 ± 2	0.026	23.14 <sup>+0.05</sup> <sub>-0.06</sub>	0.942 <sup>+0.010</sup> <sub>-0.024</sub>	27.13 <sup>+0.08</sup> <sub>-0.08</sub>	2.66 <sup>+0.10</sup> <sub>-0.10</sub>	257	0.00	-13.54	<sup>a</sup> , <sup>A</sup>
NGC 4068	13.19	201 ± 2	0.022	24.14 <sup>+0.02</sup> <sub>-0.02</sub>	1.056 <sup>+0.005</sup> <sub>-0.007</sub>	28.20 <sup>+0.06</sup> <sub>-0.06</sub>	4.36 <sup>+0.12</sup> <sub>-0.12</sub>	281	0.00	-15.10	<sup>a</sup> , <sup>C</sup>
NGC 4163	13.63	162 ± 5	0.020	23.31 <sup>+0.02</sup> <sub>-0.02</sub>	1.144 <sup>+0.004</sup> <sub>-0.005</sub>	27.35 <sup>+0.06</sup> <sub>-0.06</sub>	2.96 <sup>+0.08</sup> <sub>-0.08</sub>	163	0.00	-13.81	<sup>a</sup> , <sup>H</sup>
UGC A276	15.86	285 ± 5	0.020	23.35 <sup>+0.07</sup> <sub>-0.08</sub>	1.033 <sup>+0.030</sup> <sub>-0.057</sub>	27.34 <sup>+0.10</sup> <sub>-0.09</sub>	2.93 <sup>+0.13</sup> <sub>-0.12</sub>	288	0.00	-11.56	<sup>g</sup> , <sup>E</sup>
NGC 4214	10.24	291 ± 5	0.022	23.31 <sup>+0.06</sup> <sub>-0.06</sub>	1.652 <sup>+0.014</sup> <sub>-0.045</sub>	27.26 <sup>+0.05</sup> <sub>-0.04</sub>	2.84 <sup>+0.06</sup> <sub>-0.06</sub>	295	0.01	-17.13	<sup>c</sup> , <sup>F</sup>
UGC 7298	15.95	174 ± 2	0.023	24.17 <sup>+0.29</sup> <sub>-0.23</sub>	0.992 <sup>+0.043</sup> <sub>-0.138</sub>	28.16 <sup>+0.23</sup> <sub>-0.30</sub>	4.28 <sup>+0.46</sup> <sub>-0.59</sub>	256	0.00	-12.31	<sup>a</sup> , <sup>A</sup>
NGC 4244	10.88	248 ± 17	0.021	24.16 <sup>+0.09</sup> <sub>-0.10</sub>	1.206 <sup>+0.051</sup> <sub>-0.074</sub>	28.19 <sup>+0.12</sup> <sub>-0.11</sub>	4.34 <sup>+0.24</sup> <sub>-0.21</sub>	260	0.68	-18.08	<sup>c</sup> , <sup>B</sup>
UGC 7559	14.12	217 ± 17	0.014	24.31 <sup>+0.05</sup> <sub>-0.05</sub>	0.956 <sup>+0.019</sup> <sub>-0.018</sub>	28.32 <sup>+0.08</sup> <sub>-0.08</sub>	4.61 <sup>+0.16</sup> <sub>-0.16</sub>	230	0.00	-14.26	<sup>d</sup> , <sup>B</sup>
UGC 7577	12.95	206 ± 2	0.020	23.08 <sup>+0.03</sup> <sub>-0.03</sub>	1.049 <sup>+0.007</sup> <sub>-0.008</sub>	27.06 <sup>+0.06</sup> <sub>-0.06</sub>	2.58 <sup>+0.08</sup> <sub>-0.08</sub>	251	0.00	-14.20	<sup>a</sup> , <sup>A</sup>
NGC 4449	10.06	202 ± 33	0.019	24.15 <sup>+0.06</sup> <sub>-0.06</sub>	1.170 <sup>+0.026</sup> <sub>-0.055</sub>	28.11 <sup>+0.09</sup> <sub>-0.09</sub>	4.19 <sup>+0.17</sup> <sub>-0.17</sub>	250	0.07	-18.21	<sup>a</sup> , <sup>B</sup>
UGC 7605	14.76	310 ± 2	0.014	24.30 <sup>+0.08</sup> <sub>-0.08</sub>	0.899 <sup>+0.026</sup> <sub>-0.032</sub>	28.32 <sup>+0.10</sup> <sub>-0.10</sub>	4.61 <sup>+0.22</sup> <sub>-0.21</sub>	317	0.00	-13.62	<sup>d</sup> , <sup>A</sup>
IC 3687	13.79	350 ± 33	0.020	24.08 <sup>+0.06</sup> <sub>-0.05</sub>	0.956 <sup>+0.014</sup> <sub>-0.012</sub>	28.08 <sup>+0.08</sup> <sub>-0.08</sub>	4.12 <sup>+0.15</sup> <sub>-0.15</sub>	377	0.00	-14.37	<sup>a</sup> , <sup>B</sup>
KK 166	17.62		0.015	24.12 <sup>+0.26</sup> <sub>-0.30</sub>	1.144 <sup>+0.104</sup> <sub>-0.055</sub>	28.10 <sup>+0.31</sup> <sub>-0.26</sub>	4.17 <sup>+0.60</sup> <sub>-0.50</sub>		0.00	-10.54	<sup>f</sup>
M 94	8.74	308 ± 8	0.018	24.29 <sup>+0.04</sup> <sub>-0.03</sub>	2.106 <sup>+0.033</sup> <sub>-0.045</sub>	28.14 <sup>+0.07</sup> <sub>-0.08</sub>	4.25 <sup>+0.15</sup> <sub>-0.16</sub>	352	0.14	-19.62	<sup>f</sup> , <sup>C</sup>
IC 4182	12.02	321 ± 2	0.014	24.21 <sup>+0.04</sup> <sub>-0.04</sub>	1.431 <sup>+0.015</sup> <sub>-0.012</sub>	28.15 <sup>+0.07</sup> <sub>-0.07</sub>	4.26 <sup>+0.14</sup> <sub>-0.14</sub>	357	0.00	-16.19	<sup>a</sup> , <sup>G</sup>
UGC 8215	16.03	224 ± 2	0.011	24.17 <sup>+0.05</sup> <sub>-0.06</sub>	1.093 <sup>+0.012</sup> <sub>-0.042</sub>	28.24 <sup>+0.08</sup> <sub>-0.08</sub>	4.44 <sup>+0.16</sup> <sub>-0.16</sub>	303	0.00	-12.25	<sup>h</sup> , <sup>A</sup>
UGC 8308	15.45	150 ± 2	0.010	24.07 <sup>+0.21</sup> <sub>-0.24</sub>	0.969 <sup>+0.022</sup> <sub>-0.116</sub>	28.08 <sup>+0.25</sup> <sub>-0.22</sub>	4.14 <sup>+0.47</sup> <sub>-0.42</sub>	230	0.00	-12.68	<sup>a</sup> , <sup>A</sup>
UGC 8320	12.97	191 ± 8	0.015	24.11 <sup>+0.07</sup> <sub>-0.07</sub>	0.914 <sup>+0.031</sup> <sub>-0.037</sub>	28.12 <sup>+0.09</sup> <sub>-0.09</sub>	4.20 <sup>+0.17</sup> <sub>-0.17</sub>	270	0.00	-15.21	<sup>a</sup> , <sup>D</sup>
UGC 8331	14.46	262 ± 5	0.009	24.14 <sup>+0.03</sup> <sub>-0.03</sub>	1.072 <sup>+0.008</sup> <sub>-0.009</sub>	28.22 <sup>+0.06</sup> <sub>-0.06</sub>	4.40 <sup>+0.13</sup> <sub>-0.13</sub>	348	0.00	-13.80	<sup>a</sup> , <sup>H</sup>
NGC 5204	11.73	201 ± 2	0.013	24.31 <sup>+0.18</sup> <sub>-0.18</sub>	1.117 <sup>+0.024</sup> <sub>-0.024</sub>	28.30 <sup>+0.19</sup> <sub>-0.19</sub>	4.57 <sup>+0.40</sup> <sub>-0.40</sub>	339	0.11	-16.73	<sup>c</sup> , <sup>C</sup>
UGC 8508	14.12	57 ± 2	0.015	23.12 <sup>+0.05</sup> <sub>-0.05</sub>	0.923 <sup>+0.016</sup> <sub>-0.026</sub>	27.13 <sup>+0.08</sup> <sub>-0.08</sub>	2.67 <sup>+0.09</sup> <sub>-0.09</sub>	181	0.00	-13.07	<sup>a</sup> , <sup>A</sup>
UGC 8638	14.44	276 ± 2	0.013	24.11 <sup>+0.03</sup> <sub>-0.03</sub>	1.122 <sup>+0.005</sup> <sub>-0.005</sub>	28.17 <sup>+0.06</sup> <sub>-0.06</sub>	4.31 <sup>+0.13</sup> <sub>-0.13</sub>	275	0.00	-13.79	<sup>d</sup> , <sup>A</sup>
UGC 8651	14.22	214 ± 2	0.006	23.36 <sup>+0.03</sup> <sub>-0.03</sub>	1.004 <sup>+0.014</sup> <sub>-0.012</sub>	27.45 <sup>+0.07</sup> <sub>-0.07</sub>	3.10 <sup>+0.10</sup> <sub>-0.09</sub>	284	0.00	-13.26	<sup>e</sup> , <sup>A</sup>
UGC 8760	14.47	188 ± 2	0.016	23.51 <sup>+0.04</sup> <sub>-0.04</sub>	1.037 <sup>+0.024</sup> <sub>-0.029</sub>	27.58 <sup>+0.07</sup> <sub>-0.07</sub>	3.28 <sup>+0.10</sup> <sub>-0.11</sub>	254	0.00	-13.18	<sup>e</sup> , <sup>A</sup>
UGC 8833	15.30	221 ± 2	0.012	23.48 <sup>+0.05</sup> <sub>-0.05</sub>	1.077 <sup>+0.011</sup> <sub>-0.011</sub>	27.55 <sup>+0.08</sup> <sub>-0.07</sub>	3.24 <sup>+0.11</sup> <sub>-0.11</sub>	280	0.00	-12.30	<sup>e</sup> , <sup>A</sup>
KK 230	17.50	63 ± 2	0.014	22.46 <sup>+0.26</sup> <sub>-0.14</sub>	0.979 <sup>+0.022</sup> <sub>-0.025</sub>	26.55 <sup>+0.15</sup> <sub>-0.27</sub>	2.04 <sup>+0.14</sup> <sub>-0.25</sub>	127	0.00	-9.11	<sup>i</sup> , <sup>A</sup>
UGC 9128	14.38	160 ± 2	0.023	22.71 <sup>+0.04</sup> <sub>-0.04</sub>	0.922 <sup>+0.067</sup> <sub>-0.100</sub>	26.79 <sup>+0.07</sup> <sub>-0.07</sub>	2.28 <sup>+0.08</sup> <sub>-0.07</sub>	180	0.00	-12.51	<sup>d</sup> , <sup>A</sup>

Notes: <sup>\*</sup> Links for photometry: <sup>a</sup>Makarova, 1999 [12]; <sup>b</sup>Taylor et al., 2005 [13]; <sup>c</sup>Vaucouleurs et al., 1991 [14]; <sup>d</sup>Makarova et al., 1998 [5]; <sup>e</sup>Makarova et al., 2009 [15]; <sup>f</sup>Karachentsev et al., 2004 [16]; <sup>g</sup>Jerjen et al., 2001 [17]; <sup>h</sup>Bremnes et al., 1999 [18]; <sup>i</sup>Karachentsev et al., 2013 (in press).  
<sup>\*\*</sup> Links for the line-of-sight velocity measurements: <sup>A</sup>Begum et al., 2008 [19]; <sup>B</sup>Kovač et al., 2009 [20]; <sup>C</sup>Springob et al., 2005 [21]; <sup>D</sup>Stil and Israel, 2002 [22]; <sup>E</sup>Huchtmeier and Richter, 1986 [23]; <sup>F</sup>Huchtmeier and Seiradakis, 1985 [24]; <sup>G</sup>Tift and Cocke, 1988 [25]; <sup>H</sup>Simpson and Gottesman, 2000 [26].  
<sup>\*\*\*</sup> TRGB location, measured in the F814W<sub>TRGB</sub> filter.  
<sup>\*\*\*\*</sup> For virtually all cases we mean the value of (F814W-F606W)<sub>TRGB</sub>, with the exception of the NGC4214 galaxy, for which the color (F814W-F555W)<sub>TRGB</sub> was used.

the galaxy; (12) references to the photometry and line-of-sight velocities of galaxies. The total apparent magnitude of the galaxy, TRGB and the average color of RGB stars in the cut-off region was not corrected for galactic extinction. Note that these measurements are part of a much broader program of uniform distance measurements to the nearby, mostly dwarf galaxies via the TRGB

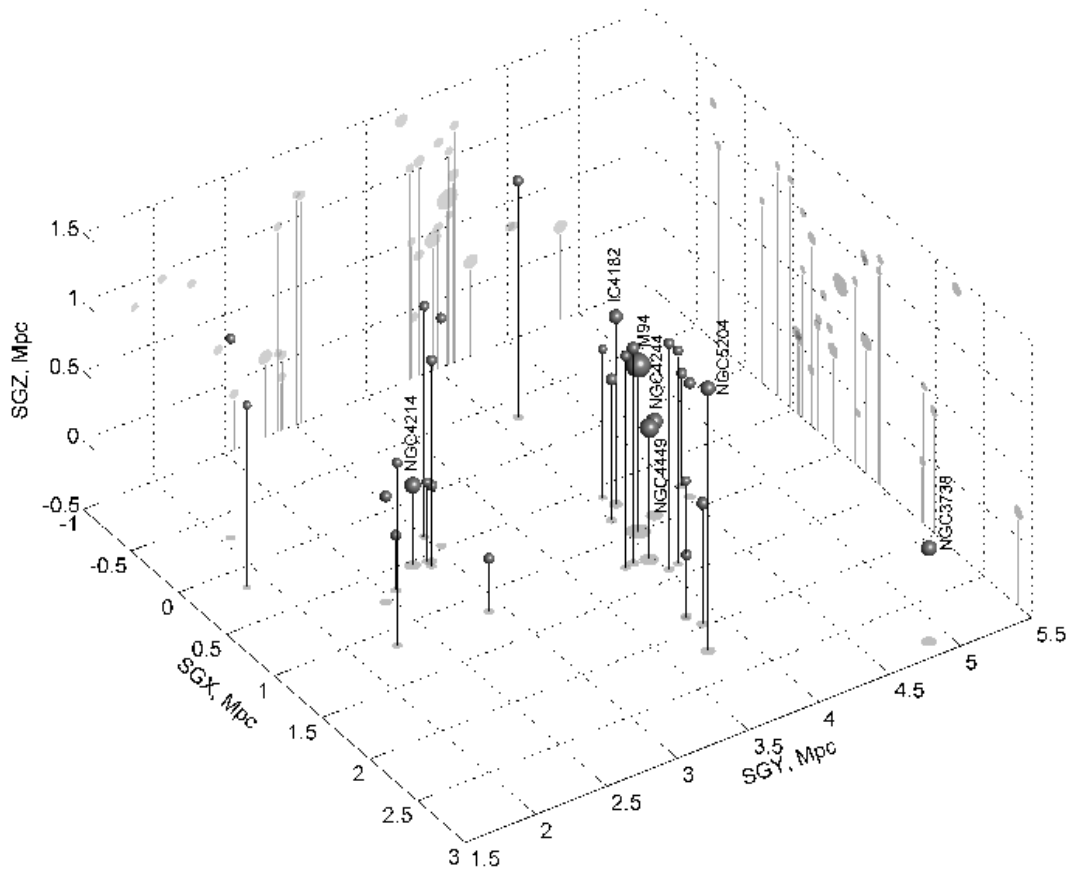


FIG. 5: A three-dimensional structure of the Canes Venatici I cloud. The sphere size is inversely proportional to the absolute magnitude of the galaxies. The names are denoted for the brightest galaxies with  $M_B < -16^m$ .

method using TRGBT00L [32].<sup>1</sup>

### A. Distance to M 94

M 94 is a giant spiral galaxy, which is located within the CVn I cloud and could be claimed as its gravitating center. Thus, it is very important to estimate the exact photometric distance to this object. M 94 was resolved into individual stars for the first time in the course of our SNAPshot observations with the HST/WFPC2 (Prop. 8601). The distance modulus, estimated from the tip of the red giant branch based on the results of photometry of the images is  $28.34 \pm 0.29$  [7]. However, the exposures with WFPC2 (600-s in the F606W filter and 600-s in the F814W filter) yield a

<sup>1</sup> <http://edd.ifa.hawaii.edu/>

sufficiently dense stellar field, while the tip of the red giant branch is located only  $1^m$  above the photometric limit. The estimate of the photometric distance in giant galaxies encounters a number of technical difficulties due to the presence of internal absorption and high surface brightness. We have determined the distance to M 94, using deeper exposures, obtained with the HST/ACS (Prop. 10,523). Three fields of M 94, located far from the center of the galaxy, were observed within this project, and hence the effect of the above-mentioned difficulties is minimized.

The luminosity function of RGB stars in the M 94 galaxy appears to be much more complex than that for the normal dwarf galaxies. It has a long, extended plateau near the cut-off. This is probably related with the complex history of star formation and metal enrichment in M 94. This behavior of the luminosity function differs from a simple power law, which usually describes the red giant branch, therefore making it impossible to use the maximum likelihood technique for determining the TRGB in the M 94 galaxy. We have thus used the classical edge detection technique, described by Sakai et al. [33] and the same up-to-date TRGB method calibrations [11] as for the other galaxies.

Our measurements give the distance modulus of  $28.14 \pm 0.08$  and the distance to the giant spiral M 94  $D = 4.25 \pm 0.15$  Mpc. This value has a better accuracy and is in a good agreement both with the earlier estimate and with the estimates made by Radburn-Smith et al. [34] from the same images. The latest work gives a distance modulus amounting to  $28.17 \pm 0.13$ .

## B. Distance to NGC 5204

Active star formation is underway in the center of the NGC 5204 galaxy. It is extremely difficult to determine the distance to the galaxy because of a dense stellar field, a large number of young stars and the proximity of the TRGB to the photometric limit (about  $1^m$ ). To get rid of “contamination” of the diagram by a large number of young stars, and to avoid the excessive influence of the nearby stellar fields on the photometry results, we have selected only the stars, located far from the star forming regions. This approach has allowed us to increase the contrast of the red giant branch and determine the position of its cut-off. As in the case M 94, we used the edge detection method. The measured distance modulus to the NGC 5204 galaxy is  $(m - M)_0 = 28.30 \pm 0.19$ , which is in excellent agreement with the estimate  $(m - M)_0 = 28.34 \pm 0.27$ , obtained in [7] based on the same data.

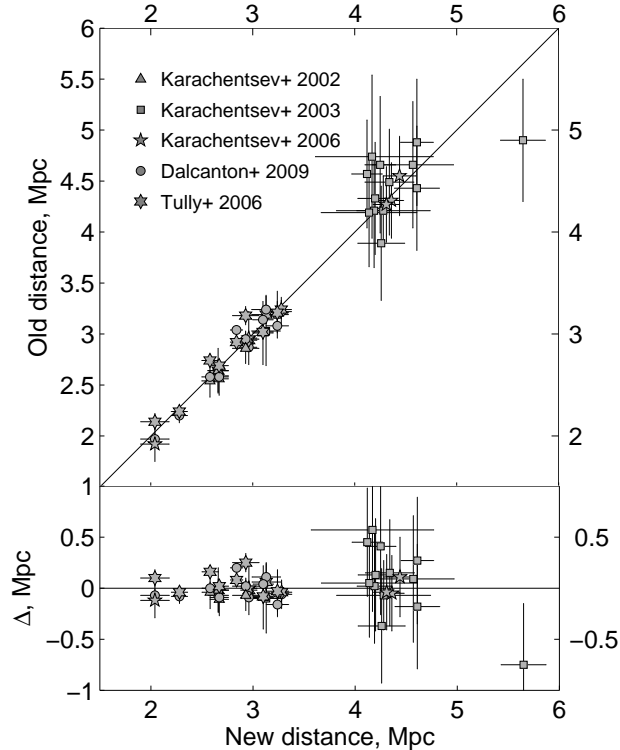


FIG. 6: A comparison of the distances obtained in this work, with earlier measurements. The data are taken from [7, 35–38].

## V. DISCUSSION AND CONCLUSIONS

Figure 5 demonstrates the spatial distribution of galaxies, obtained from our distance measurements in supergalactic coordinates. The sphere size is proportional to the logarithm of the galaxy luminosity. The concentration of galaxies around M94, the brightest member of the CVnI, is clearly visible here.

A comparison of our distance estimates with the measurements by other authors [7, 35–38] shows a very good agreement with a generally better accuracy (Fig. 6). The increased measurement accuracy is due both to the deeper observations of the same galaxies, carried out at a later time, and the use of a more refined technique of distance estimation.

The Hubble diagram of the recession of galaxies in the direction of the Canes Venatici is shown in Fig. 7. Note that in the previous study of the structure of this cloud of galaxies, this region looks much more “fuzzy” (Fig. 6 in [7]), which did not allow to make a conclusion on the virialized state of this group of galaxies. The higher quality of observations allows us to identify an area of chaotic motions around the center of the system. The group of galaxies around M94 is characterized by

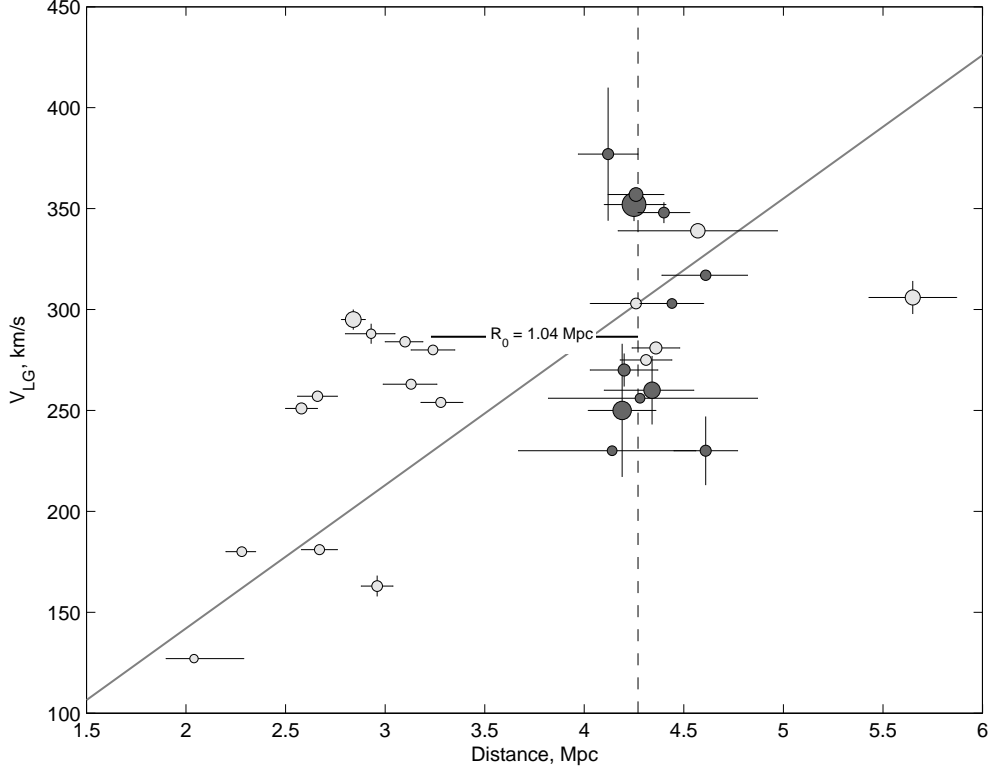


FIG. 7: The velocity–distance diagram for the galaxies in the Canes Venatici region. The linear Hubble law with  $H_0 = 71 \text{ km}/(\text{s}\times\text{Mpc})$  is depicted by the solid line. The galaxies within 1 Mpc from the center of the system are marked in dark gray. The median average distance of the central concentration is shown by the dashed line.

a median velocity of  $V_{\text{LG}} = 287 \text{ km/s}$ , median distance of  $D = 4.28 \text{ Mpc}$ , the line-of-sight-velocity dispersion of  $\sigma = 51 \text{ km/s}$ , corrected for the measurement errors, the mean projected distance from the galactic center of the system of  $\langle R \rangle = 455 \text{ kpc}$ , and the total luminosity of  $L_B = 1.61 \times 10^{10} L_{\odot}$ . The mass of the system, estimated by the virial theorem amounts to  $M_{\text{vir}} = 1.93 \times 10^{12} M_{\odot}$ , which corresponds to the mass–luminosity ratio of  $(M/L)_{\text{vir}} = 120 (M/L)_{\odot}$ . The projection mass estimate [39] of this system is  $M_p = 2.56 \times 10^{12} M_{\odot}$  and the corresponding mass–luminosity ratio amounts to  $(M/L)_p = 159 (M/L)_{\odot}$ . Note, however, that the crossing time of the CVn I cloud of galaxies,  $T_{\text{cr}} = R_h/\sigma = 6.5 \text{ Gyr}$  makes up about half the age of the Universe  $T = 13.7 \text{ Gyr}$ . Therefore, the issue of the system’s proximity to the steady state requires further consideration, and one should use the virial theorem to estimate the mass of the system with caution.

As noted in [7], almost all the galaxies, located closer than the central concentration CVn I have positive peculiar velocities and form the characteristic “wave,” caused by the infall of matter onto the massive clusters of galaxies (see, e.g., [40]). Unfortunately, the current data on the distances

of galaxies, located behind the studied CVn I cloud, does not allow to unambiguously claim that there is a similar infall of matter on the opposite side of the group, although some hints imply this. According to our data, only the NGC 3738 galaxy has a fairly deep CMD to measure the distance of 5.65 Mpc. Apparently, this galaxy “falls” onto the CVn I cloud from the opposite side and has a large negative peculiar velocity of  $V_{\text{pec}} = -95$  km/s. If we suppose that the observed distribution of galaxies on the Hubble diagram at the distances of less than 3.5 Mpc is due to the gravitational effect of the group of galaxies around M 94, we can estimate the radius of the zero velocity sphere  $R_0 = 1.04 \pm 0.15$  Mpc as the mean between the forward and reverse regressions of the velocity and distance of galaxies. It corresponds to the mass  $M_{R_0} = 2.38 \times 10^{12} M_{\odot}$  (formula from [40]). This value is in a good agreement with the projection mass estimate. The analysis of peculiar velocities of field galaxies is independent of the virial theorem by the system mass measurement method. A more accurate mass estimate of the CVn I cloud should include a simulation of the distribution of galaxies by peculiar velocities and their spatial distribution.

Our mass–luminosity estimate,  $(M/L)_p = 159 (M/L)_{\odot}$  for the CVn I cloud of galaxies greatly exceeds the typical ratio  $M/L_B \sim 30$  for the nearby groups of galaxies, such as the Local Group ( $M/L_B = 15\text{--}20$ ) and M 81 group ( $M/L_B = 19\text{--}32$ ) [41]. Note that compared with the well-known nearby groups, such as the Local Group ( $L_B = 10.1 \times 10^{10} L_{\odot}$ ), M 81 ( $L_B = 6.1 \times 10^{10} L_{\odot}$ ) and Centaurus A ( $L_B = 5.5 \times 10^{10} L_{\odot}$ ), the CVn I cloud of galaxies ( $L_B = 1.61 \times 10^{10} L_{\odot}$ ) contains about 4–5 times less luminous matter, and M 94 is at least 1<sup>m</sup> fainter than any other central galaxy of these groups [41]. However, the concentration of galaxies in the Canes Venatici may have a comparable total mass.

The catalog of groups of galaxies in the Local Supercluster [42] has demonstrated that the mean density of gravitating matter on the scale of 80 Mpc is about 2.5 times smaller than the cosmological constant  $\Omega_m = 0.27$ . One possible explanation for this striking difference between the global and local estimates of density of the Universe can be the presence of a significant proportion of dark matter outside the virialized regions associated with luminous matter. Such “dark aggregates” can be quite numerous. For example, Tully et al. [37] have identified the associations of nearby dwarf galaxies by the high-precision photometric distances obtained by the Hubble Space Telescope. Moreover, it was noted in this paper that on the scale of up to 3 Mpc, with the exception of the KKR 25 galaxy, all the known galaxies are either combined in groups, or associations. Such rarefied structures may possess the mass–luminosity ratios in the range from 100 to 1000  $(M/L)_{\odot}$ . It was shown in [43] that the groups consisting of dwarf galaxies only may be numerous, and they have higher mass–luminosity ratios than the typical galaxy groups in the Local Supercluster. It is



possible that the cloud of galaxies in the Canes Venatici is in fact one of these concentrations of dark matter, where the ratio of dark to luminous matter significantly exceeds a similar proportion in the typical groups of galaxies.

### Acknowledgments

The authors thank prof. I. D. Karachentsev for constructive discussions. This work was supported by the RFBR grant no. 11-02-00639 and the grant of the Ministry of Education and Science of the Russian Federation no. 8523. The study was also supported by the program of the Physical Sciences Division RAS PSD-17 “Active Processes in Galactic and Extragalactic Objects.” We made use of the HyperLEDA database (<http://leda.univ-lyon1.fr>).

- 
- [1] I. D. Karachentsev, *Astrophysics* **2**, 39 (1966).
  - [2] G. de Vaucouleurs, *Nearby Groups of Galaxies* (University of Chicago Press, Chicago, 1975), p. 557.
  - [3] L. N. Makarova, I. D. Karachentsev, and T. B. Georgiev, *Astron. Lett.* **23**, 378 (1997).
  - [4] N. A. Tikhonov and I. D. Karachentsev, *A&AS* **128**, 325 (1998).
  - [5] L. Makarova, I. Karachentsev, L. O. Takalo, et al., *A&AS* **128**, 459 (1998).
  - [6] I. D. Karachentsev and I. O. Drozdovsky, *A&AS* **131**, 1 (1998).
  - [7] I. D. Karachentsev, M. E. Sharina, A. E. Dolphin, et al., *A&A* **398**, 467 (2003).
  - [8] K. Kovač, T. A. Oosterloo, and J. M. van der Hulst, *MNRAS* **400**, 743 (2009).
  - [9] S. S. Kaisin and I. D. Karachentsev, *A&A* **479**, 603 (2008).
  - [10] D. Makarov, L. Makarova, L. Rizzi, et al., *AJ* **132**, 2729 (2006).
  - [11] L. Rizzi, R. B. Tully, D. Makarov, et al., *Astrophys. J.* **661**, 815 (2007).
  - [12] L. Makarova, *A&AS* **139**, 491 (1999).
  - [13] V. A. Taylor, R. A. Jansen, R. A. Windhorst, et al., *Astrophys. J.* **630**, 784 (2005).
  - [14] G. de Vaucouleurs, A. de Vaucouleurs, H. G. Corwin, et al., *VizieR Online Data Catalog* **7155**, 0 (1995).
  - [15] L. Makarova, I. Karachentsev, L. Rizzi, et al., *MNRAS* **397**, 1672 (2009).
  - [16] I. D. Karachentsev, V. E. Karachentseva, W. K. Huchtmeier, and D. I. Makarov, *AJ* **127**, 2031 (2004).
  - [17] H. Jerjen, R. Rekola, L. Takalo, et al., *A&A* **380**, 90 (2001).
  - [18] T. Bremnes, B. Binggeli, and P. Prugniel, *A&AS* **137**, 337 (1999).
  - [19] A. Begum, J. N. Chengalur, I. D. Karachentsev, et al., *MNRAS* **386**, 1667 (2008).
  - [20] K. Kovač, T. A. Oosterloo, and J. M. van der Hulst, *MNRAS* **400**, 743 (2009).
  - [21] C. M. Springob, M. P. Haynes, R. Giovanelli, and B. R. Kent, *ApJS* **160**, 149 (2005).

- [22] J. M. Stil and F. P. Israel, *A&A* **389**, 29 (2002).
- [23] W. K. Huchtmeier and O. G. Richter, *A&AS* **63**, 323 (1986).
- [24] W. K. Huchtmeier and J. H. Seiradakis, *A&A* **143**, 216 (1985).
- [25] W. G. Tifft and W. J. Cocke, *ApJS* **67**, 1 (1988).
- [26] C. E. Simpson and S. T. Gottesman, *AJ* **120**, 2975 (2000).
- [27] A. E. Dolphin, *PASP* **112**, 1383 (2000).
- [28] A. E. Dolphin, *MNRAS* **332**, 91 (2002).
- [29] D. J. Schlegel, D. P. Finkbeiner, and M. Davis, *Astrophys. J.* **500**, 525 (1998).
- [30] I. D. Karachentsev and D. A. Makarov, *AJ* **111**, 794 (1996).
- [31] I. D. Karachentsev, D. I. Makarov, and E. I. Kaisina, *AJ* , 2013 (in press).
- [32] B. A. Jacobs, L. Rizzi, R. B. Tully, et al., *AJ* **138**, 332 (2009).
- [33] S. Sakai, B. F. Madore, and W. L. Freedman, *Astrophys. J.* **461**, 713 (1996).
- [34] D. J. Radburn-Smith, R. S. de Jong, A. C. Seth, et al., *ApJS* **195**, 18 (2011).
- [35] I. D. Karachentsev, M. E. Sharina, D. I. Makarov, et al., *A&A* **389**, 812 (2002).
- [36] I. D. Karachentsev, A. Dolphin, R. B. Tully, et al., *AJ* **131**, 1361 (2006).
- [37] R. B. Tully, L. Rizzi, A. E. Dolphin, et al., *AJ* **132**, 729 (2006).
- [38] J. J. Dalcanton, B. F. Williams, A. C. Seth, et al., *ApJS* **183**, 67 (2009).
- [39] J. Heisler, S. Tremaine, and J. N. Bahcall, *Astrophys. J.* **298**, 8 (1985).
- [40] I. D. Karachentsev, O. G. Kashibadze, D. I. Makarov, and R. B. Tully, *MNRAS* **393**, 1265 (2009).
- [41] I. D. Karachentsev, *AJ* **129**, 178 (2005).
- [42] D. Makarov and I. Karachentsev, *MNRAS* **412**, 2498 (2011).
- [43] D. I. Makarov and R. I. Uklein, *Astrophysical Bulletin* **67**, 135 (2012).